# Research on Aggregated Modeling of Wind Farms Considering Dynamic Coupling Characteristics and Stability Optimization in Weak Grid Environments

Zhan Zhao[1,*] and Ziyang Chen[2]

[1]*School of Control and Computer Engineering, North China Electric Power University, Beijing, China*
[2]*School of Information Technology, Beijing University of Technology, Beijing, China*
*E-mail: zhuliu107@163.com*
[*]*Corresponding Author*

Received 14 November 2025; Accepted 11 January 2026

## Abstract

The application of Grid-Forming (GFM) and Grid-Following (GFL) controllers has effectively enhanced the strength of increasingly weakened power system. However, the inherent high-order and nonlinear characteristics of wind farm models pose numerous challenges to the simulation and analysis of the dynamic stability of modern power systems.

To address these challenges, this paper proposes an innovative aggregated modeling approach for wind farms, which enables large-scale simulation and serves as a powerful tool for modern power system stability analysis. Based on the distinct Thevenin equivalent circuits of GFL and GFM units, this study introduces their respective rotor current and stator voltage weighting coefficients for the aggregation of wind turbines operating under different control modes. The constructed model can accurately represent wind farm dynamic characteristics across varying grid strengths and fault conditions. To

*Strategic Planning for Energy and the Environment, Vol. 45_2,* 403–428.
doi: 10.13052/spee1048-5236.4525

verify the proposed model's effectiveness, this paper compares the accuracy of the modal aggregation method against other multi-machine representation methods under Fault Ride-Through (FRT) conditions. Results demonstrate a significant reduction in errors between the proposed aggregation model and detailed model in the pre-fault, fault-on and post-fault stages. In addition, the aggregated model is utilized to investigate the port characteristics of wind farms with different GFM-GFL unit proportions. It is shown that a reasonable increase in the proportion of GFM and GFL units can significantly enhance the operational stability of wind turbines under low Short-Circuit Ratio (SCR) conditions, and effectively expand their stable operating range in weak grid environments.

**Keywords:** Wind farm, grid-forming, grid-following, aggregation modeling, short-circuit ratio.

## 1 Introduction

Wind energy, as a clean and renewable energy source, plays a pivotal role in the global energy transition. Driven by technological progress and policy support, the wind energy sector has grown rapidly, becoming vital for climate action and carbon neutrality [1]. According to GWEC's 2025 Global Wind Energy Report, global new wind installations hit 117 GW in 2024, with cumulative capacity surpassing 1,000 GW by 2025 [2], a significant increase compared with 2023. However, the power fluctuations of wind turbine generators may induce grid voltage fluctuations and harmonic pollution. During grid faults, turbines must maintain Low-Voltage Ride-Through (LVRT) capability to avoid disconnection and prevent system collapse [3].

The control modes of wind turbine generators can be classified into two categories: Grid-Following active support control based on current sources and Grid-Forming control based on voltage sources. GFL units, relying on Phase-Locked Loops (PLLs) for grid synchronization, are vulnerable to disconnection under faults, lacking voltage and frequency support [4]. By contrast, GFM units can independently build voltage and maintain synchronization, enabling stable operation under weak/off-grid conditions. GFM units can also offer rapid power adjustment, inertia response, and primary frequency regulation to suppress system oscillations [5]. As renewable power systems evolve, hybrid GFL and GFM wind turbine operation will emerge as a trend, balancing efficient power output under strong grid conditions with

independent operation capabilities in weak/off-grid scenarios, and provide flexibility across diverse grid environments [6].

Currently, wind farm modeling mainly includes detailed and aggregated models. Detailed models include all turbines and transmission lines. With the increase of units, the order and time domain simulation time will increase. Aggregated models consider the wind farm as a whole, using a single or multiple equivalent models to simulate its steady-state or dynamic characteristics, which reduce complexity and computational load [7]. Reference [8] proposes a practical four-machine equivalent method for Doubly-Fed Induction Generator (DFIG) wind turbines to minimize errors, enabling applicability of aggregated models for short-term transient grid fault analysis. However, significant discrepancies emerge between the aggregated model and detailed models under dynamic fault ride-through conditions. Reference [9] proposes a classification method, which can reflect the transient voltage characteristics of DFIG according to the impact during fault. The partition of wind farm is achieved by adopting clustering algorithm similarly. Nevertheless, the indicators selected above cannot reflect the active power dynamic response characteristics roundly. In terms of clustering metrics, one approach uses environmental factors, such as turbine layout, wind speed [10], and Jensen wake model [11], while another relies on electrical characteristics [12], such as DFIG power, transient voltage, and current in Reference [13]. However, when significant and frequent variations in wind speed occur among wind turbines within a large-scale wind farm, it can lead to frequent alterations in the clustering result. The second category focuses on transient characteristics [14, 15].

According to the preceding description, existing methods show errors in electromagnetic transient LVRT scenarios. To address this issue, this paper analyzes the error sources and proposes an innovative aggregation method: Based on the current source characteristics of GFL wind turbines and the voltage source characteristics of GFM wind turbines, this paper introduces rotor current weight coefficients for GFL and voltage weight coefficients for GFM to effectively aggregate turbines with different control modes. Subsequently, this paper conducts a rigorous verification of the method's performance under fault ride-through characteristics, proving that it fully meets the accuracy requirements of electromagnetic transient simulation. Using this model, this paper further studies the influence of different proportional configuration of GFM and GFL units on the port characteristics of the wind farm under weak grid conditions, and carries out the corresponding stability analysis.

## 2 Description of GFL and GFM DFIG Wind Turbines

### 2.1 Modeling of a DFIG Wind Turbine

Figure 1 illustrates the grid-connected system structure of DFIG wind turbines, including a Doubly-Fed Induction Generator, a Machine Side Converter (MSC), a Direct Current (DC) link, a Grid Side Converter (GSC), a step-up transformer, and some cables. The DFIG's rotor windings are controlled by a back-to-back converter system, which consists of a MSC and a GSC. These converters are connected via a DC link to control the rotor windings. By adjusting the control strategies of both converters, the DFIG enables flexible regulation of active and reactive power injected into the grid. The DFIG is connected to the AC grid through a step-up transformer. The AC grid models as a fixed voltage source behind an equivalent impedance, which comprises resistance $R_g$ and reactance $X_g$ [16].

### 2.2 DFIG-GFL Control Strategies (MSC, GSC)

The concept of GFL refers to a control strategy in which the converter operates synchronously with the grid by keeping its voltage and frequency consistent with that of the grid.

In a DFIG operating under GFL, MSC needs to be synchronized with stator voltage and frequency to independently regulate active and reactive power. The Phase Locked Loop is used to eliminate the interference of the stator voltage vector, and the stator active and reactive power are proportional to the rotor currents $i_{rq}, i_{rd}$ respectively, so the cascaded rotor current controller can be used to effectively regulate the current.

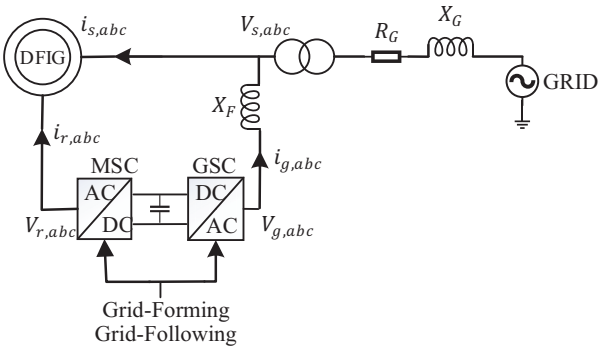


**Figure 1** Grid-connected DFIG model.

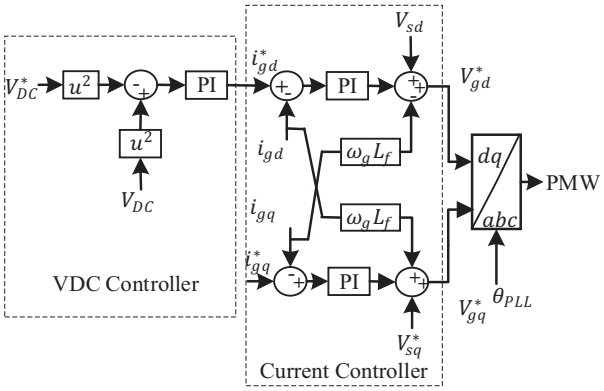


**Figure 2** DC-link voltage controller and current controller.

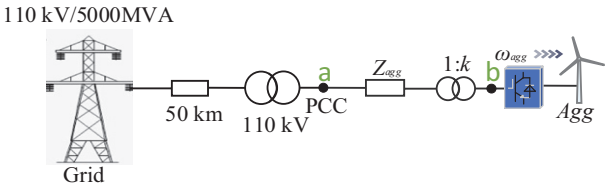


**Figure 3** GFL wind farm integration system.

In a DFIG, GSC primarily maintains DC-link voltage stability, which can be achieved by controlling output power. In the GFL mode, this can be accomplished by decoupling the active and reactive power control.

In the d-q synchronous reference frame, PLL is used to align the voltage component $V_{s,q} = 0$. Under this condition, the active power and reactive power will be proportional to the d-axis components $i_{g,d}$ and q-axis components $i_{g,q}$ of the grid current [17]. In order to realize the DC bus voltage control, an outer loop controller can be cascaded outside the current controller. Its structure is shown in Figure 2.

In the grid-connected system of the grid-following wind farm shown in Figure 3, the voltage and frequency of the grid-connected point 'a' are regulated by a power plant controller (PPC), and the Static Var Generator (SVG) compensates the reactive power to maintain the voltage stability of point 'a'. When the grid is strong, the system can operate stably. As the proportion of wind farms increases, the power grid strength weakens accordingly, and the Short-Circuit Ratio (SCR) falls below 3. The voltage at point 'b' on the individual unit side becomes critical. When the voltage at point 'a' is

maintained at 1 p.u. (per unit value), after passing through the transformer and line impedance, the voltage at point 'b' drops below 0.8 p.u., which is lower than the LVRT threshold. This leads to instability in the wind farm, repeatedly triggering the ride-through protection and causing oscillations. Therefore, it is necessary to employ GFM units to support the terminal voltage of the wind farm, and form a hybrid wind farm with GFL units to meet the needs of stable operation of the system under weak grid conditions.

## 2.3 DFIG-GFM Control Strategies (APC, RPC, and Virtual Damping)

The GFM concept refers to the capability of the converter or the DFIG machine to autonomously generate the required voltage and frequency through self-synchronizing energy exchange mechanisms.

$$P_s \approx \frac{V_s V_G}{X_{eq}}\delta = P_{\max}\delta, \quad Q_s \approx \frac{V_s(V_s - V_G)}{X_{eq}} \tag{1}$$

Equation (1) reveals the direct relationship between power angle ($\delta$) and active power ($P_s$), voltage difference ($V_s - V_G$) and reactive power ($Q_s$), forming the core control strategy of GFM topology, which can accurately regulate active power, reactive power. This concept is realized into two external control loops shown in Figure 4: the Active Power Controller (APC) loop controls the frequency of the converter to adjust the active power, and the Reactive Power Controller (RPC) loop regulates the terminal voltage amplitude to affect the reactive power, thereby realize grid synchronization.

The APC loop regulates active power by adjusting the output converter frequency via PI control, which minimizes the error between measured and reference power to modulate output. When the MSC operates, the DFIG in maximum power point tracking (MPPT) mode adjusts active power reference based on wind speed and turbine speed, ensuring optimal output under variable conditions, and the PI controller will self-synchronize with the power

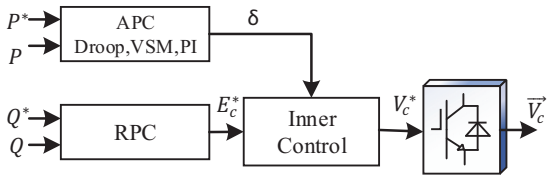


**Figure 4** GFM control diagram.

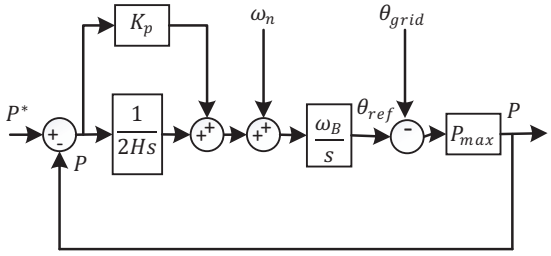


**Figure 5** Active power synchronization control strategy.

grid and adjust according to the MPPT power. For the GSC, APC stabilizes DC-link voltage, with the PI controller continuously regulating power flow to maintain voltage within the desired range. As shown in Figure 5, the PI control parameters can be adjusted so that the integrated gain is equivalent to the virtual inertia.

The RPC loop affects the reactive power by adjusting the terminal voltage of MSC or GSC, thereby realize grid synchronization. This adjustment is implemented using a PI controller, as described in the following equation:

$$V_s^* = V_n + \left(K_{pq} + \frac{K_{iq}}{s}\right)(Q_s^* - Q_s) \tag{2}$$

Where: $Q_s$ is the reactive power reference, $Q_s^*$ is the reactive power measurement, and $V_n$ is the feedforward term of the nominal voltage. A Virtual Resistor (VR) strategy is used in RPC to reduce the vulnerability of GFM converters to Sub-Synchronous Resonance (SSR). As shown in Figure 6, the virtual resistor suppresses all non-fundamental frequency components through a Second Order Generalized Integrator (SOGI) and an open-loop gain without affecting the operation of the system under steady-state conditions.

Under weak grid conditions, the GFM control strategy for the MSC in DFIG wind turbines exhibits superior stability and adaptability, effectively mitigating disturbances such as grid phase shifts, series capacitive compensation, and voltage dips, while maintaining enhanced damping and robustness under low SCR scenarios. Critically, the MSC exerts a dominant influence on system stability, determining system behavior independently, thereby enabling GFM-based DFIGs to actively support grid stability.

However, to suppress low-frequency oscillations, GFM-DFIGs require virtual damping implementation [18], which increases control algorithm complexity and results in relatively slower dynamic responses. Conversely, when operating in GFL mode, wind turbines demonstrate stable performance

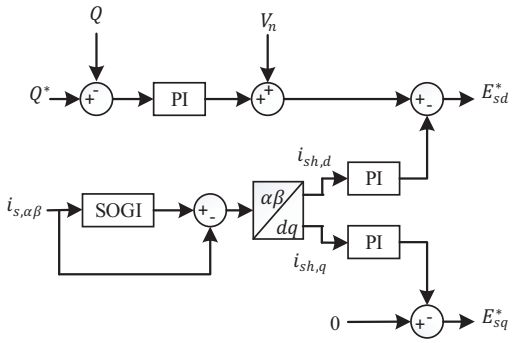


**Figure 6** Reactive power control strategy.

under high SCR and sufficient inertia conditions. During grid frequency or voltage fluctuations, GFL-based turbines can rapidly adjust output power, providing fast and stable responses.

## 3 Aggregated Modeling Approach for Wind Farms Considering Dynamic Coupling Characteristics

To thoroughly investigate the characteristics of hybrid wind farms composed of GFM and GFL wind turbines under weak grid conditions while reducing the order of wind farm models and computational burden, aggregated modeling is required to simulate their dynamic behaviors [19]. This section incorporates dynamic coupling characteristics of wind farms and proposes a modal correction approach, introducing rotor currents of GFL turbines and stator voltages of GFM turbines as weighting coefficients to achieve effective aggregation of wind turbine generators with distinct control modalities.

### 3.1 Weighted Current Aggregation Approach for GFL Wind Turbines

Each Wind Turbine Generator (WTG) is characterized by a set of small-signal equations that constitute the d-axis and q-axis circuits shown in Figure 7. The research objective is to find an equivalent WTG with the same structural characteristics of the individual WTGs, so that its dynamic characteristics can be close to the dynamic performance of the entire wind farm from the perspective of the grid [20]. Therefore, a set of small signal equations and d-axis and q-axis circuits similar to single wind turbines should also be provided for the equivalent wind turbine with a grid. From a control perspective, the GFL

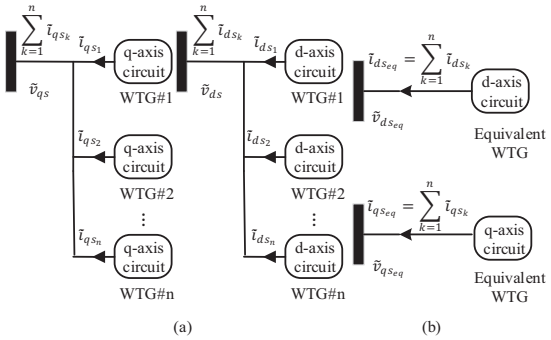


**Figure 7** (a) The d-q axis circuit of GFL wind farm (b) Equivalent model of d-q axis circuit.

turbine can be modeled as a controllable current source with current-tracking capability.

$$\tilde{v}_{ds_{eq}} = \tilde{v}_{ds}, \quad \tilde{v}_{qs_{eq}} = \tilde{v}_{qs}$$
$$\tilde{i}_{ds_{eq}} = \sum_{k=1}^{n} \tilde{i}_{ds_k}, \quad \tilde{i}_{qs_{eq}} = \sum_{k=1}^{n} \tilde{i}_{qs_k} \tag{3}$$

Consequently, the contribution of each individual WTG to the grid-injected current of the entire wind farm can be quantified. The proposed method calculates equivalent WTG parameters through weighted averaging of individual WTG parameters, where the weights are determined by each WTG's current contribution to the grid. As shown in Figure 7, both wind farm and individual WTG currents can be projected onto d-axis and q-axis circuits. To simplify the derivation, the d-q reference frame is rotated to a d′–q′ frame such that the total grid-injected current contains no q'-axis component. Rearrange these currents in the new d′–q′ frame where:

$$\sum_{k=1}^{n} \tilde{i}'_{qs_k} = 0 \tag{4}$$

where $\delta_0$ represents the phase difference between the two d-q reference axes as shown in Figure 8. The weighting factor for the dynamic equations of the m-th WTG is defined as:

$$\mu_m = \frac{\tilde{i}'_{ds_m}}{\sum_{k=1}^{n} \tilde{i}'_{ds_k}} \tag{5}$$

The equivalent unit and its control parameters can be derived using the weighted average method based on per-unit values of individual wind turbine

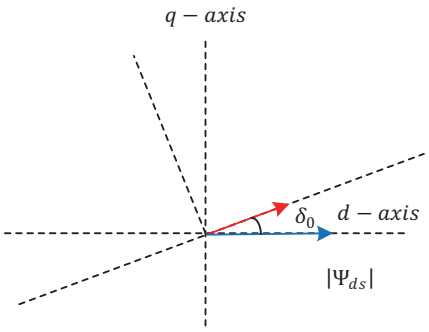


**Figure 8** Rotate the d-q reference frame by an angle of $\delta_0$.

parameters, while the apparent power of the equivalent WTG is obtained by summing the apparent powers of all WTGs in the wind farm. For instance, the equivalent inductance $L_{meq}$ can be calculated as follows:

$$L_{m_{eq}} = \sum_{k=1}^{n} \mu_k L_{m_k}, \quad \sum_{k=1}^{n} \mu_k = 1 \tag{6}$$

## 3.2 Weighted Voltage Support Aggregation Approach for GFM Wind Turbines

The GFM unit can be regarded as a controllable voltage source providing voltage support to the power grid. When the voltage of the wind farm deviates, the $\Delta U_k$ support capacity of each wind turbine supports the $\Delta U$ of the wind farm together. Similar to aggregation with GFL wind turbines, the contribution of each individual WTG to voltage deviation compensation $\Delta u$ within the wind farm can be quantified. Equivalent WTG parameters were calculated by the weighted average of the WTG parameters, where these weights were determined by the contribution of each WTG support voltage deviation.

$$\Delta U_{ds_{eq}} = \sum_{k=1}^{n} \Delta U_{ds_k}, \quad \Delta U_{qs_{eq}} = \sum_{k=1}^{n} \Delta U_{qs_k} \tag{7}$$

As illustrated in Figure 9, the voltage deviations of both the wind farm and individual WTGs can be projected to d-and q-axis circuits. Analogous to the aggregation methodology for GFL wind turbines, we perform a coordinate rotation from the d-q reference frame to the d′–q′ reference frame, ensuring

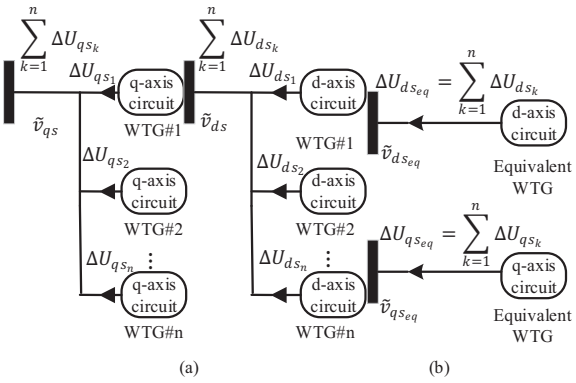


**Figure 9** (a) The d-q axis circuit of GFM wind farm (b) equivalent model of d-q axis circuit.

that the total voltage deviation $\Delta U$ injected into the grid contains no q′-axis component. After realignment in this new d′–q′ coordinate system:

$$\sum_{k=1}^{n} \Delta U'_{qs_k} = 0 \tag{8}$$

The weighting factor for the dynamic equation of the m-th WTG is defined as:

$$H_m = \frac{\Delta U'_{ds_m}}{\sum_{k=1}^{n} \Delta U'_{ds_k}} \tag{9}$$

Equivalent unit and control parameters can be obtained by the weighted average method of the standard value of each parameter of each wind turbine.

In summary, in the proposed method, the parameters of the equivalent WTG can be obtained by performing a Weighted Dynamics (WD) analysis of the equivalent reduced-order system $\dot{X}_{eq} = [A_{eq}]X_{eq}$ derived from the detailed wind farm model defined by $\dot{X} = [A_w]X$, Where $X$ is the full-order system state, $A_w$ is the detailed system matrix, $X_{eq}$ is the state of a single equivalent WTG model, and $A_{eq}$ is the system parameter and equilibrium point.

## 4 Simulation Results

### 4.1 Wind Farm System Structure and Parameter Setting

Figure 10 illustrates the equivalent aggregation process of 50 grid-connected wind turbines in a wind farm: the detailed models of 10 GFL wind turbines

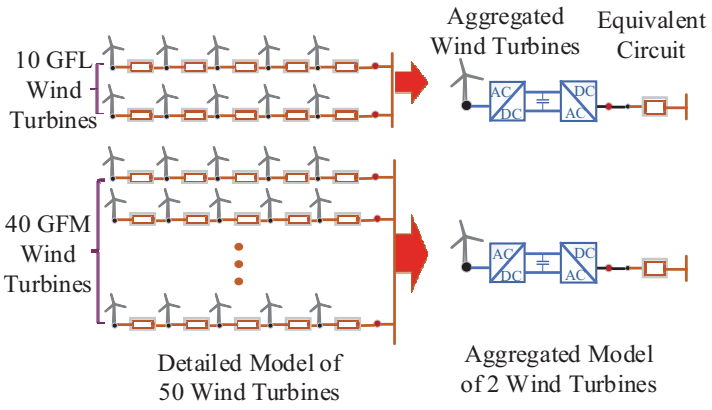


**Figure 10** The equivalent aggregation process of wind farms.

**Table 1** WTG parameters in machine base

| Parameter Category | Parameter Name | Abbreviation | Value |
|---|---|---|---|
| WTG System | Rated Power | $P_{rated}$ | 5 MW |
| | Wind Speed | – | 15 m/s |
| | Blade Length | $R$ | 40.05 m |
| | Number of Pole Pairs | $n_{pp}$ | 2 |
| | Gearbox Ratio | – | 51.78 |
| Performance | Optimal Tip Speed Ratio | $\lambda_{opt}$ | 8.10 |
| | Normalized Synchronous Speed | $\omega_s$ | 1 p.u. |
| Electrical Parameters | Mutual Inductance | $L_m$ | 4 p.u. |
| | Stator Inductance | $L_{ss}$ | $1.01 \times L_m$ |
| | Rotor Inductance | $L_{rr}$ | $1.005 \times L_{ss}$ |
| | Stator Resistance | $R_s$ | 0.005 p.u. |
| | Rotor Resistance | $R_r$ | $1.1 \times R_s$ |
| Inertia & Stiffness | Turbine Inertia | $H_t$ | 4 s |
| | Generator Inertia | $H_g$ | 0.4 s |
| | Shaft Stiffness | $k$ | 0.03 p.u./ele.rad |
| | Damping Coefficient | $c$ | 0.01 p.u.s/ele.rad |
| Filter Components | Capacitance | – | 0.0113 p.u. |
| | Inductance | – | 0.01 p.u. |
| | Resistance | – | 0.0001 p.u. |

and 40 GFM wind turbines are aggregated into two equivalent wind turbine models. Each aggregated wind turbine is connected to the power grid through equivalent lines. The parameter settings for the wind turbines are shown in Table 1 [21].

## 4.2 Error Analysis of Multiple Modeling Methods in Transient Processes

Figure 11 presents a comparison of the accuracy between the aggregated model and the detailed model in terms of active and reactive power under a LVRT scenario. From the perspective of the active power curve, at 0.5 s of the voltage sag in segment A, the Mean Squared Error (MSE) in per-unit values between the aggregated model and the detailed model is 0.20. During the power recovery phase, the error further increases, reaching an MSE of 0.31 in Section B.

Regarding the reactive power curve, although the degree of agreement between the aggregated model and the detailed model is better compared to the active power curve, errors still persist. Specifically, the error in Section A is relatively small, with an MSE value of 0.15. However, as the dynamic process progresses, the error in Section B increases, with an MSE of 0.21.

It can thus be seen that during the transient process of LVRT, the aggregated model exhibits unsatisfactory accuracy in simulating both active and reactive power, with non-negligible errors existing when compared to the detailed model.

Figure 12 is a sample diagram of wind speed distribution of wind farm. In the diagram, the x-axis represents sample points, ranging from 0 to 100, while the y-axis indicates the serial numbers of wind turbines, with a range from 0 to 150. Each point represents the wind speed value of the corresponding wind turbine at a specific sample time, and collectively they form a two-dimensional wind speed distribution matrix, illustrating the variations in wind speed at multiple wind turbines and different sample times.

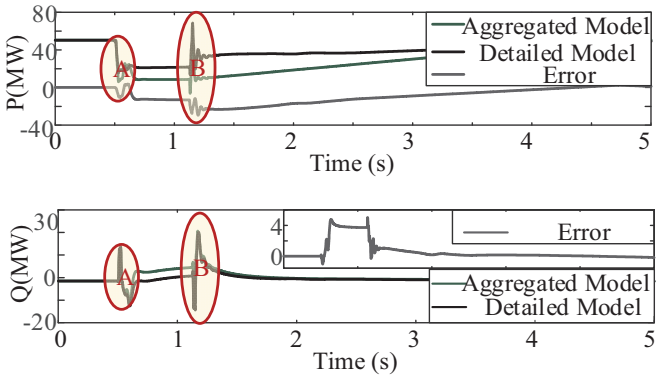


**Figure 11** Comparison of dynamic responses in active and reactive power of wind farms.

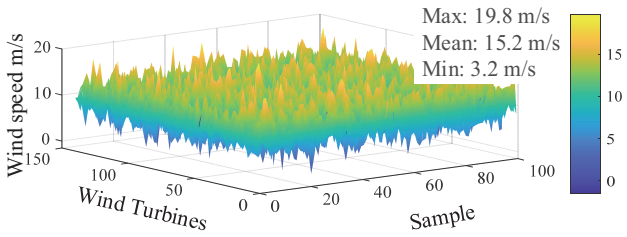


**Figure 12** Wind speed stochastic distribution diagram of wind farms.

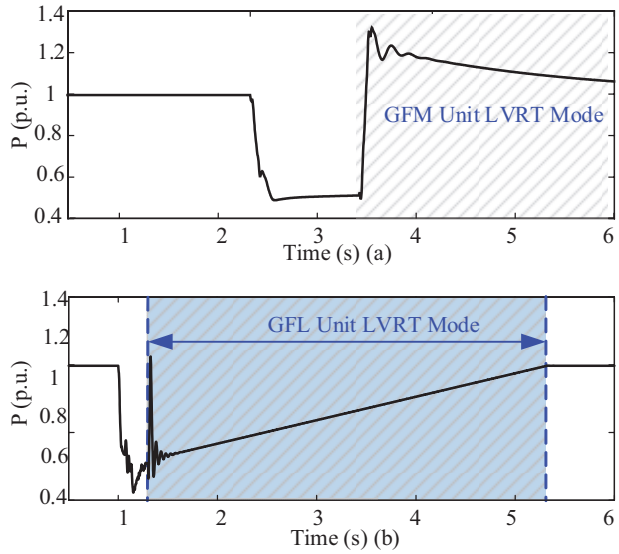


**Figure 13** (a) FRT characteristics of GFM units (b) FRT characteristics of GFL units.

Wind speed varies greatly across sample points and turbine locations, spanning a wide range. Some areas approach the maximum value of 19.8 m/s and are depicted in yellow, while others approach the minimum value of 3.2 m/s and are shown in blue. This indicates the presence of distinct high-wind-speed and low-wind-speed zones within the test scenario, with an average wind speed of 15.2 m/s. There are pronounced fluctuations in wind speed. The wind speed of some turbines varies violently, and the curve fluctuates greatly, while some are relatively smooth. It reflects the instability and randomness of wind speed, which may be influenced by various factors, such as terrain and meteorological conditions, highlighting the uncertainty and complexity of wind speed distribution.

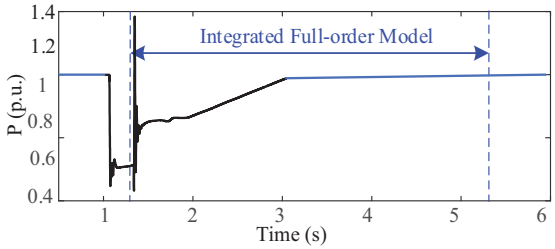


**Figure 14** FRT characteristics of wind farm.

Figure 13 displays the fault ride-through characteristic curves of GFM units and GFL units respectively, while Figure 14 shows the FRT characteristic curve of the combined full-order model. At 1 s, both the GFM and GFL wind turbines experience a voltage sag and subsequently initiate LVRT. During this process, the active power of both types of wind turbines drops to 0.48 p.u. However, there are significant differences in their power recovery performances: the active power of the GFM wind turbine rapidly increases, achieving effective active power compensation in just 0.27 s. In contrast, the active power curve of the GFL wind turbines first undergoes 0.3 s of oscillation, then rose slowly, and then returned to 1 p.u. after 4.2 s. Thus, it is evident that DFIG wind turbines with different control strategies exhibit substantial differences in their operational modes.

When the two types of wind turbines are combined to a full-order model, the active power waveform exhibits a unique variation trend: the power waveform oscillates in the time period of 1–1.3 s, then gradually recovers in 1.3–3 s, and finally stabilizes at 1 p.u. Due to the uncertainty of wind speed and the differences in the configuration methods between GFM and GFL wind turbines, the dynamic characteristics of the combined full-order model are different from those of GFM and GFL units. As a result, transient errors are inevitably generated between the aggregated model and the detailed model during the transient process.

### 4.3 Applicability Verification of Aggregation Model Under Low Voltage Fault Through (LVRT) Condition

This paper compares the dynamic characteristics of active and reactive power across three different methods, as illustrated in Figure 15. Methods 1 and 2 are multi-machine representations, utilizing 3-machine and 5-machine configurations, respectively. Although all three methods match accurately in the steady state, deviations arise for Methods 1 and 2 during transient periods.

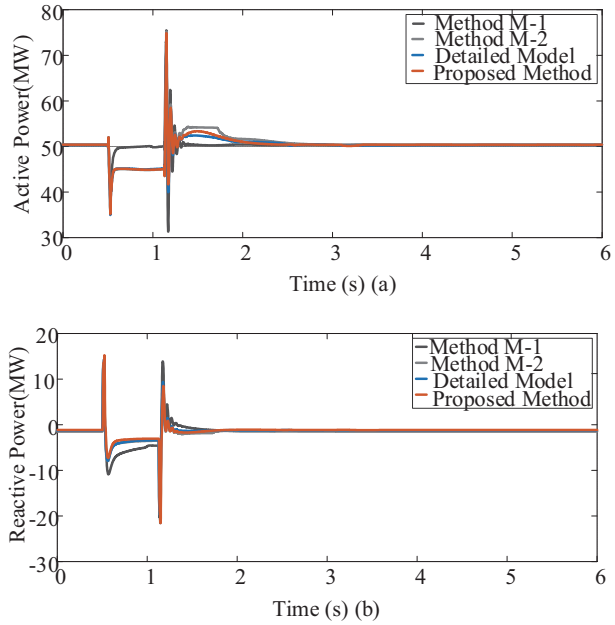


**Figure 15** Comparison of active and reactive power fault recovery characteristics of the proposed aggregation model, existing aggregation model and detailed model.

The error MSE values for active power are 0.4 and 0.39, respectively, while those for reactive power are 0.3 and 0.29. This phenomenon indicates that transient error persists even when a greater number of wind turbines are used to represent a wind farm. The mechanism of transient error is discontinuous and unexplained. In this paper, a modal modification method is used to improve the accuracy of the model, and the MSE value is reduced to 0.03. Figure 15 demonstrates the accuracy of the proposed method before, during, and after faults, with MSE values of 0.0003, 0.07, and 0.00019, respectively. These results validate the effectiveness of the method in capturing the transient characteristics of wind turbines, making it suitable for research on weak grid system enhancement.

## 4.4 Research on the Enhancement of Weak Grid Systems

### 4.4.1 Calculation of SCR and weak grid system configuration

In this study, to simulate the weak grid environment, precise configuration of grid strength is required, and the line impedance is the key determinant of SCR. The lower the SCR, the weaker the system. By flexibly adjusting

the reactance and impedance values of the equivalent line, the SCR can be effectively regulated, thereby establishing weak grid conditions that meet the research requirements.

The Short-Circuit Ratio is defined as the ratio of the short-circuit capacity of the DC conversion bus to the rated DC power [22]. It is determined that the ratio of reactance to resistance is 3, $X = 3R$:

$$SCR = \frac{S_{sc}}{S_{WTG}} = \frac{\frac{U_{sc}^2}{|Z_{sc}|}}{S_{WTG}} = \frac{\frac{U_{sc}^2}{\sqrt{R^2+X^2}}}{S_{WTG}} = \frac{U_{sc}^2}{S_{WTG}R\sqrt{1+\left(\frac{X}{R}\right)^2}} \tag{10}$$

Where $S_{sc}$ is the short-circuit capacity, $S_{WTG}$ is the rated capacity, $U_{sc}$ is the grid voltage, $R$ is the impedance, $X$ is the reactance, and the values of $R$ and $X$ can be obtained by calculation. The system set impedance $Z_{sc}$ and the reference impedance $Z_{base}$ are calculated as follows:

$$|Z_{sc}| = \frac{U_{sc}^2}{S_{sc}} = \sqrt{R^2 + X^2} = R\sqrt{1 + \left(\frac{X}{R}\right)^2} \tag{11}$$

$$|Z_{base}| = \frac{U_{sc}^2}{S_{LC}} \tag{12}$$

Where, $S_{LC}$ represents the line capacity. Through calculation, the values of resistance $(R)$, reactance $(X)$, and the impedance angle $(\phi)$ can be obtained:

$$R = \frac{|Z_{sc}|}{\sqrt{1+\left(\frac{X}{R}\right)^2}} = \frac{|Z_{sc}|}{\sqrt{1+3^2}} = \frac{|Z_{sc}|}{\sqrt{10}} \tag{13}$$

$$\phi = \tan^{-1}\left(\frac{X}{R}\right) = \tan^{-1} 3 \tag{14}$$

Calculate the corresponding impedance scale value:

$$R_{p.u.} = \frac{R}{|Z_{base}|}, \quad X_{p.u.} = \frac{X}{|Z_{base}|} \tag{15}$$

The reactance and impedance values corresponding to the SCR are obtained, and use them to configure equivalent lines in wind power grid-connection systems under different short-circuit ratio conditions.

The validity of the aggregated model must be verified under varying grid strength conditions. In the dynamic process of the power grid, SCR is

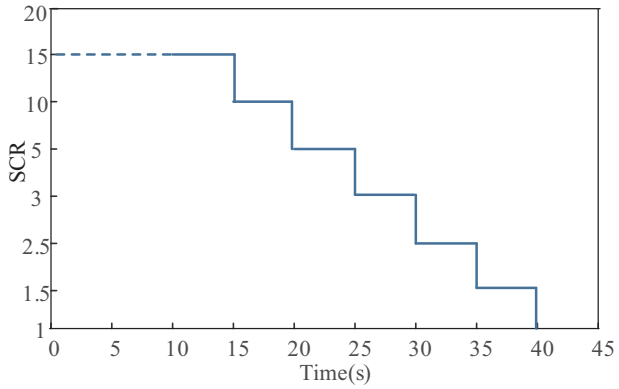


**Figure 16** Diagram of system SCR under stepwise variation conditions.

expected to exhibit a stepwise downward gradient. As shown in Figure 16, the system environment changes from a strong grid to a weak grid over time, with SCR decreasing stepwise from 15 to 1. In this dynamic change, especially when the short-circuit ratio changes lead to unstable LVRT of wind turbines, the aggregation model can better fit the actual situation, so as to verify its effectiveness under different grid strengths.

### 4.4.2 Influence of configuration ratio of GFM wind turbines in a wind farm on system stability

Research indicates that when grid strength exhibits a gradient decline, the deployment of GFM wind turbines significantly enhances system stability [23]. This is primarily attributed to their capability of providing reactive power support, enabling effective active and reactive power output even under weak grid conditions [24]. This section employs a modal aggregation approach to construct a hybrid wind farm model comprising GFM and GFL wind turbine units. The analysis focuses on the dynamic characteristic variations of the wind farm's grid-connected port when the penetration ratio of grid-forming units reaches 20% and 60%, respectively.

Figure 17 shows the active and reactive power response curves of the dynamic characteristics of wind turbine units as the SCR varies, when the proportion of grid-forming wind turbines in the wind farm is 20%. From 0 to 25 s, the wind turbine units operate stably in a strong grid environment. Between 25 and 30 s, with the system SCR in the range of 3 to 2.5, the wind turbine units demonstrate a certain capability to operate in a weak grid, and both the active and reactive power curves remain dynamically stable. After

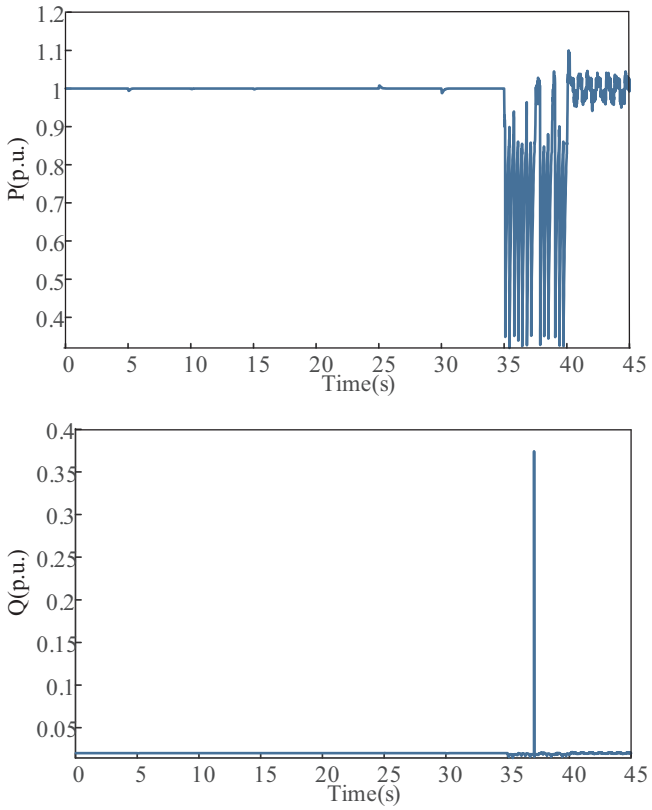


**Figure 17** Dynamic active and reactive power responses of the units under varying SCR with 20% GFM wind turbines integration.

35 s, when the SCR drops below 1.5, the wind turbine units are unable to operate stably under the corresponding weak grid conditions. Both the active and reactive power curves exhibit oscillations, and the system demonstrates dynamic instability.

Figure 18 shows the voltage response curve of the dynamic characteristics of the unit as the SCR varies, when the proportion of grid-shaped fans is 20%. From 0 to 25 s, the system port voltage gradually decreases with the decrease of power grid strength. Between 25 and 30 s, with the system SCR in the range of 3 to 2.5, the GFM wind turbines provide voltage support, and the voltage curve remains dynamically stable in this period. The SCR continues to decrease. After 35 s, when the SCR is lower than 1.5, the port voltage begins to diverge and oscillate, indicating dynamic instability.

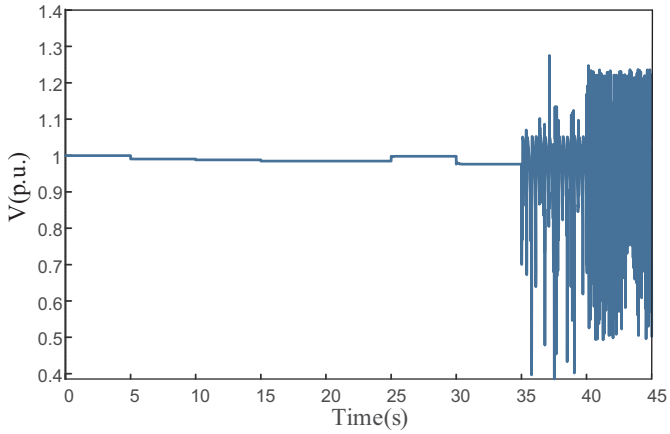


**Figure 18** Dynamic voltage response at units terminals under varying SCR with 20% GFM wind turbines integration.

In conclusion, the SCR of 3 and 1.5 is the watershed to judge the stability of the system. Configuring a certain proportion of GFM units can effectively support power stability during the process of a decline of the SCR of the system.

Figure 19 illustrates the active and reactive power responses of the dynamic characteristics of wind turbine units as the SCR varies, when the proportion of GFM wind turbines in the wind farm reaches 60%. From 0 to 35 s, as the system SCR gradually decreases from 15 to 1.5, the active power curve remains dynamically stable. The reactive power curve rises significantly at 35 s, increasing from 0.025 p.u. to 0.175 p.u. This indicates that a high proportion of GFM wind turbines provides substantial reactive power support in a weak grid environment where the SCR drops to 1.5. After 40 s, when the SCR further decreases to below 1, both curves exhibit noticeable oscillations, demonstrating dynamic instability.

Figure 20 displays the dynamic response of the system terminal voltage as the SCR varies, when the proportion of GFM wind turbines in the wind farm is 60%. It can be observed that the voltage drops significantly at 35 s, when the SCR decreases to 1.5, but then quickly recovers to 1p.u. The GFM units provide reactive power support under weak grid conditions (SCR = 1.5) by dynamically adjusting the emission and absorption of reactive power, thereby maintaining the stability of the terminal voltage. After 40 s, when the SCR further drops below 1, the voltage curve exhibits oscillatory divergence, indicating dynamic instability.

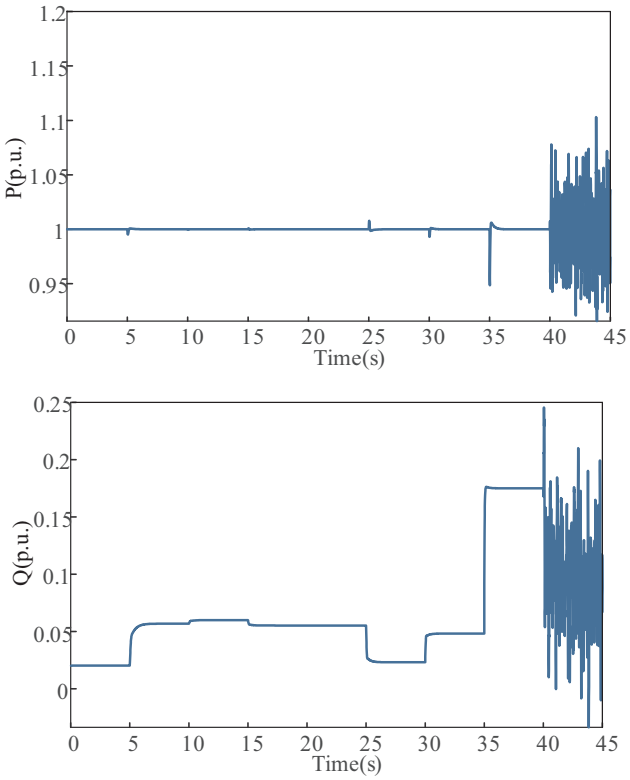


**Figure 19** Dynamic active and reactive power responses of the units under varying SCR with 60% GFM wind turbines integration.

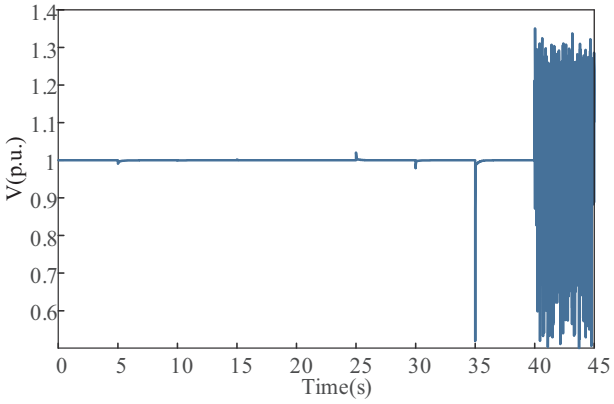


**Figure 20** Dynamic voltage response at units terminals under varying SCR with 60% GFM wind turbines integration.

Research shows that by reasonably increasing the ratio of GFM to GFL wind turbine units, the operational stability of wind farm under low SCR conditions can be significantly enhanced, and their stable operating range in weak grid environments can be effectively expanded.

## 5 Conclusion

To address the challenge of analyzing the dynamic stability of wind farms with hybrid GFM and GFL wind turbines operating under weak grid conditions, this study innovatively proposes a wind farm aggregation modeling method that accounts for dynamic coupling characteristics. It fully preserves the current-source characteristics of GFL units and voltage-source characteristics of GFM units, enabling accurate aggregation of turbines with different control modes and effectively resolving the large-error issue of traditional models in electromagnetic transient LVRT scenarios. The established model provides an efficient and reliable tool for simulating the dynamic characteristics of wind farms in weak grid environments.

The aggregation model was employed to investigate the impact of GFM turbine configuration ratios on system stability. Results indicate that a reasonable increase in the proportion of GFM turbines (e.g., raising it to 60%) can significantly enhance the operational stability of wind turbines under SCR conditions by strengthening reactive power support capability, effectively expanding their stable operation range in weak grid environments. Meanwhile, an SCR of 1.5 serve as a critical threshold for stable system operation; when the SCR falls below this value and the GFM turbine proportion is insufficient, the system tends to suffer from oscillatory instability. The conclusions offer important technical references for the planning and design, control strategy optimization, and stable operation of wind farms. Future research may further explore the coordinated optimization strategies between GFM and GFL turbines to better adapt to complex and variable weak grid conditions.

## References

[1] Da, C., Zhang, T., Ma, G., Wang, J., and Liu, R. (2023). "Evaluation Method of Efficient Power Marketing Strategy Based on Multi-dimensional Clustering Algorithm," *Strategic Planning for Energy & the Environment*, 42(3).

[2] GWEC. Global wind report 2025[R/OL]. [2025-04-23]. https://gwec.net/global-wind-report-2025/.

[3] Zhang, Q. (2025). "Research on the Construction of Short-term Prediction Model of Wind Farm Output Power Based on Deep Learning Model," *Strategic Planning for Energy & the Environment*, 44(1).

[4] B. Wen, D. Boroyevich, R. Burgos, P. Mattavelli and Z. Shen, "Analysis of D-Q Small-Signal Impedance of Grid-Tied Inverters," in *IEEE Transactions on Power Electronics*, vol. 31, no. 1, pp. 675–687, Jan. 2016.

[5] Y. Jin, Z. Zhang and Z. Xu, "Proportion of Grid-forming Wind Turbines in Hybrid GFM-GFL Offshore Wind Farms Integrated with Diode Rectifier Unit Based HVDC System," in *Journal of Modern Power Systems and Clean Energy*, vol. 13, no. 1, pp. 87–101, January 2025.

[6] L. Zhan et al., "Transient Modeling and Postfault Stability Analysis of GFM-DFIG Considering Rotor-Side Current Limitation," in *IEEE Transactions on Power Electronics*, vol. 40, no. 9, pp. 11979–11984, Sept. 2025.

[7] H. Liu and Z. Chen, "Aggregated Modelling for Wind Farms for Power System Transient Stability Studies," 2012 *Asia-Pacific Power and Energy Engineering Conference*, Shanghai, China, 2012, pp. 1–6.

[8] W. Li, P. Chao, X. Liang, J. Ma, D. Xu and X. Jin, "A Practical Equivalent Method for DFIG Wind Farms," in *IEEE Transactions on Sustainable Energy*, vol. 9, no. 2, pp. 610–620, April 2018.

[9] J. Zou, C. Peng, H. Xu and Y. Yan, "A Fuzzy Clustering Algorithm-Based Dynamic Equivalent Modeling Method for Wind Farm With DFIG," in *IEEE Transactions on Energy Conversion*, vol. 30, no. 4, pp. 1329–1337, Dec. 2015.

[10] Y. Jin, D. Wu, P. Ju, C. Rehtanz, F. Wu and X. Pan, "Modeling of Wind Speeds Inside a Wind Farm with Application to Wind Farm Aggregate Modeling Considering LVRT Characteristic," in *IEEE Transactions on Energy Conversion*, vol. 35, no. 1, pp. 508–519, March 2020.

[11] A. P. Gupta, A. Mitra, A. Mohapatra and S. N. Singh, "A Multi-Machine Equivalent Model of a Wind Farm Considering LVRT Characteristic and Wake Effect," in *IEEE Transactions on Sustainable Energy*, vol. 13, no. 3, pp. 1396–1407, July 2022.

[12] D. Wang, Q. Zhou, W. Shen, D. Gu and X. Yang, "Research on Wind Farm Clustering Modeling for Power Grid Dynamic Equivalence," 2021 *5th International Conference on Smart Grid and Smart Cities (ICSGSC)*, Tokyo, Japan, 2021, pp. 55–60.

[13] X. Liu, Y. Zhang and H. Li, "A Novel Wind Turbines Clustering Method Based on Their Transient Voltage Characteristics," 2025 *8th International Conference on Energy, Electrical and Power Engineering (CEEPE)*, Wuxi, China, 2025, pp. 655–660.

[14] W. Zheng, J. Bu, N. Zhang, Q. Zhou and J. Liu, "Dynamic Clustering Equivalence of Wind Farms Considering Impacts of Collection Lines," 2018 *IEEE 2nd International Conference on Circuits, System and Simulation (ICCSS)*, Guangzhou, China, 2018.

[15] Z. Chen, "A dynamic equivalent aggregation method of PMSG wind farm for voltage stability study," *6th Asia Conference on Energy and Electrical Engineering (ACEEE)*, Chengdu, China, 2023, pp. 393–398.

[16] A. Paez, J. Chen, M. Schütt and H. -G. Eckel, "Comparative analysis of grid-forming and grid-following control for DFIG," *23rd Wind & Solar Integration Workshop (WIW 2024)*, Hybrid Conference, Helsinki, Finland, 2024, pp. 640–645.

[17] L. Sun and X. Zhao, "Impacts of Phase-Locked Loop and Reactive Power Control on Inertia Provision by DFIG Wind Turbine," in *IEEE Transactions on Energy Conversion*, vol. 37, no. 1, pp. 109–119, March 2022.

[18] M. Li, Z. Xie, S. Xu, S. Yang and X. Zhang, "Electromechanical Oscillation Analysis and Suppression of Grid Forming DFIG-Based Wind Turbines Under Weak Grid," in *IEEE Transactions on Energy Conversion*, vol. 40, no. 2, pp. 1365–1377, June 2025.

[19] Shang, W., Liu, Y., Zhao, L., Pan, S., and Pan, F. (2025). "Research on Power Demand Response and Operation Optimization Model in Source-grid-load-storage Integration Project," *Strategic Planning for Energy & the Environment*, 44(3).

[20] N. Shabanikia, A. A. Nia, A. Tabesh and S. A. Khajehoddin, "Weighted Dynamic Aggregation Modeling of Induction Machine-Based Wind Farms," in *IEEE Transactions on Sustainable Energy*, vol. 12, no. 3, pp. 1604–1614, July 2021.

[21] L. P. Kunjumuhammed, B. C. Pal, C. Oates and K. J. Dyke, "Electrical Oscillations in Wind Farm Systems: Analysis and Insight Based on Detailed Modeling," in *IEEE Transactions on Sustainable Energy*, vol. 7, no. 1, pp. 51–62, Jan. 2016.

[22] O. Damanik, Ö. C. Sakinci, G. Grdenić and J. Beerten, "Evaluation of the use of short-circuit ratio as a system strength indicator in converter-dominated power systems," *2022 IEEE PES Innovative Smart Grid*

*Technologies Conference Europe (ISGT-Europe)*, Novi Sad, Serbia, 2022, pp. 1–5.

[23] H. Xin, C. Liu, X. Chen, Y. Wang, E. Prieto-Araujo and L. Huang, "How Many Grid-Forming Converters Do We Need? A Perspective from Small Signal Stability and Power Grid Strength," in *IEEE Transactions on Power Systems*, vol. 40, no. 1, pp. 623–635, Jan. 2025.

[24] Duan, Q., Chao, Z., Fu, C., Zhong, Y., Zhuo, J., and Liao, Y. (2024). "Design of Short-Term Power Load Forecasting Model Based on Deep Neural Network," *Strategic Planning for Energy and the Environment*, 425–452.

## Biographies

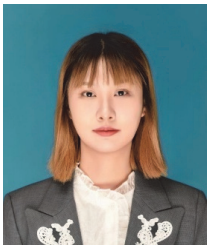

**Zhan Zhao** received the bachelor's degree in Automation from North China Electric Power University in 2022, the master's degree in Control Science and Engineering from North China Electric Power University in 2025, respectively. Her research areas include wind power generation and intelligent Control Strategy.

**Ziyang Chen** received the bachelor's degree in Software Engineering from Beijing University of Technology in 2022. He is currently employed at

a burgeoning internet company, serving as a data development engineer. His research areas include AI large-scale models and the end-to-end processing of data, which includes ETL (Extract, Transform, Load) extraction, constructing data warehouses, and subsequent data analysis. Currently, I am employed at a burgeoning internet company, serving as a Data Development Engineer.